THE EUROPEAN
PHYSICAL JOURNAL A

Separation energies of light Λ hypernuclei and their theoretical uncertainties

Hoai Le[1,a], **Johann Haidenbauer**[1,b], **Ulf-G. Meißner**[2,1,3,4,c], **Andreas Nogga**[1,4,d]

[1] Institut für Kernphysik, Institute for Advanced Simulation and Jülich Center for Hadron Physics, Forschungszentrum Jülich, 52425 Jülich, Germany

[2] Helmholtz-Institut für Strahlen- und Kernphysik and Bethe Center for Theoretical Physics, Universität Bonn, 53115 Bonn, Germany

[3] Tbilisi State University, Tbilisi 0186, Georgia

[4] CASA, Forschungszentrum Jülich, 52425 Jülich, Germany

Abstract Separation energies of light Λ hypernuclei ($A \leq 5$) and their theoretical uncertainties are investigated. Few-body calculations are performed within the Faddeev-Yakubovsky scheme and the no-core shell model. Thereby, modern and up-to-date nucleon-nucleon, three-nucleon and hyperon-nucleon potentials derived within chiral effective field theory are employed. It is found that the numerical uncertainties of the few-body methods are well under control and an accuracy of around 1 keV for the hypertriton and of better than 20 keV for the separation energies of the $^4_\Lambda$He and $^5_\Lambda$He hypernuclei can be achieved. Variations caused by differences in the nucleon-nucleon interaction are in the order of 10 keV for $^3_\Lambda$H and no more than 110 keV for $A = 4$, 5 Λ hypernuclei, when recent high-precision potentials up to fifth order in the chiral expansion are employed. The variations are smaller than the expected contributions from chiral hyperon-nucleon-nucleon forces which arise at the chiral order of state-of-the-art hyperon-nucleon potentials. Estimates for those three-body forces are deduced from a study of the truncation uncertainties in the chiral expansion.

1 Introduction

The insight into the properties of the ΛN interaction that one can gain from the available scattering experiments [1–5] is somewhat limited. Specifically, essential features like its spin dependence cannot be deduced from those data. Because of that, already at an early stage of hypernuclear physics,

measurements of light Λ hypernuclei were explored as an additional source of information. For example, the conjecture that the ΛN interaction in the spin-singlet state should be more attractive than the one in the triplet state was drawn from such analyses around 60 years ago [6–8].

Light hypernuclei continue to play an essential role in testing and improving our understanding of the hyperon-nucleon (YN) interaction. Fortunately, the theoretical and computational tools for pertinent investigations have been improved dramatically over the years. Techniques for treating few-body systems have been matured to a level that rigorous calculations with sophisticated two-body potentials, including the full complexity of YN dynamics like tensor forces or the important coupling between the ΛN and ΣN channels, have become feasible. To be concrete, binding energies of $A = 3$ and 4 hypernuclei can be obtained by solving Faddeev or Yakubovsky (FY) equations [9–11] for such YN interactions. Other *ab initio* methods like the no-core shell model (NCSM) allow one to compute even binding energies for hypernuclei beyond the s shell [12–17] and, so far, studies of hypernuclei up to $^{13}_\Lambda$C have been reported [15].

With the improvement in the methods another aspect moved into the foreground of hypernuclear studies, namely that of estimating the uncertainties of the achieved results. Of course, this concerns first of all the applied techniques themselves. However, it extends also to uncertainties due to an essential input in such microscopic calculations, the underlying nucleon–nucleon (NN) potential and possibly three-nucleon forces ($3NF$s). Only with those ingredients under control, reliable conclusions on the YN interaction to be examined can be drawn.

Bound-state calculations performed over the last two decades suggest that the Λ separation energies of light hyper-

[a] e-mail: h.le@fz-juelich.de (corresponding author)

[b] e-mail: j.haidenbauer@fz-juelich.de

[c] e-mail: meissner@hiskp.uni-bonn.de

[d] e-mail: a.nogga@fz-juelich.de

Springer

nuclei are not very sensitive to the employed NN interaction [11,18]. For example, for a high-precision NN interaction derived within chiral effective field theory (EFT) like the semi-local momentum-space-regularized (SMS) potential of fifth order (N^{4}LO) [19], the variation of the separation energy with regulator cutoffs $\Lambda_N = 400 - 550$ MeV is of the order of 100 keV for $^4_\Lambda$He/$^4_\Lambda$H [18], when combined with next-to-leading order (NLO) YN potentials derived likewise in chiral EFT. The variation has to be seen in relation to the total experimental separation energy which is 2.347 ± 0.036 MeV for the $^4_\Lambda$He (0^+) state [20]. Indeed, such a variation is within the range expected from earlier calculations based on phenomenological NN and YN interactions [11]. It was therefore very surprising that Htun et al. [21] reported an NN-interaction dependence of the hypertriton separation energy of 100 keV, i.e. of the same order as the separation energy itself. A recent more extended study by the same group found variations of around 250 keV for $A = 4$ hypernuclei and of more than 1 MeV for $^5_\Lambda$He [22]. Since the empirical $^5_\Lambda$He separation energy is 3.102 ± 0.030 MeV [20] such a value implies that the uncertainty could increase dramatically with A. It should, however, be noted that the analysis in question is limited to NN and three-nucleon (3N) forces of next-to-next-to-leading order (N^{2}LO) in the chiral expansion and to leading order (LO) with regard to the YN interaction. In the earlier work of Wirth and Roth [23] variations of ≈ 200 keV and ≈ 400 keV have been found for $^7_\Lambda$Li and $^9_\Lambda$Be, respectively, utilizing N^{3}LO and N^{4}LO NN potentials (and N^{2}LO 3NFs), but again only LO interactions for the YN system.

In the present work, we want to re-examine the uncertainties of calculations for the separation energies of light hypernuclei. One of the main motivations for the study comes from the already mentioned fact that the analysis by Gazda et al. [22] is based on two-body potentials of fairly low chiral orders, a factor which could limit its conclusiveness. As a matter of fact, and as likewise mentioned above, with regard to the NN system, potentials up to N^{4}LO [19,24] are now the standard for computations of few-nucleon systems [25]. Also, for the YN interaction, LO is no longer the state-of-art. Recently potentials up to N^{2}LO in the chiral expansion have become available [26]. Thus, contrary to the calculation in [22] where the focus was on exploring solely a large family of N^{2}LO NN and 3N potentials, called NNLO$_{sim}$ [27], we extend our analysis to variations observed when employing potentials of different chiral order, for the NN as well as the YN systems. Specifically, we consider NN potentials from LO to N^{4}LO, supplemented by 3NFs starting from N^{2}LO, and YN potentials from LO to N^{2}LO.

The paper is structured in the following way: In the subsequent section we describe the strategy of our analysis and the NN, 3N, and YN interactions used as input. In Sect. 3 uncertainties related to the applied methods for treating few-body systems are explored. Uncertainties due to the employed NN

and YN interactions are investigated in Sect. 4. The paper closes with a brief summary.

2 Strategy and input

In the uncertainty analysis for NN interactions derived within chiral EFT, several aspects have been considered such as the error due to the truncation in the chiral expansion, statistical uncertainties in the LECs of the NN contact terms, errors associated with the pion-nucleon LECs, and the role of the energy range when fitting the NN scattering data [19,27–30]. In general the uncertainty is dominated by the truncation error. Thus, in our analysis for the YN interaction the main focus will be likewise on the uncertainty due to the truncation in the chiral expansion. We employ the most advanced chiral NN potentials (N^{4}LO$^+$) of the Bochum group, which provide the presently best possible representation of the NN interaction, for the main part of our analysis. Here the $^+$ in N^{4}LO$^+$ indicates that some of the short-range operators appearing at N^{5}LO are also included, see [19].

Our study is to some extend complementary to the work of Refs. [21,22] where the focus was on a statistical exploration of effects from the nuclear interactions, based on a family of 42 NN and 3N N^{2}LO potentials. We restrict the number of variations and combinations of NN (3N) and YN potentials, in view of our limited CPU resources, and give priority to precision and reliability of the computation within the FY and the Jacobi-NCSM (J-NCSM) methods [31]. Accordingly, we perform only selective calculations with lower-order NN potentials for orientation and illustration—and also to connect with some of the results presented in Refs. [21,22]. Of course, strict compliance with the power counting would require that we treat the NN and YN systems on the same level in studies of hypernuclei, i.e. combine a LO YN potential with a LO NN potential, etc. However, we think that this procedure would provide little insight into the properties of the YN force, given the fact that we are not able to achieve the same accuracy for YN as for the NN interaction. Thus, we believe that the strategy that we follow here minimizes the bias from the NN potential and allows for the best possible estimate of the truncation error for the hypernuclear separation energies due to the YN interaction.

In the following, we evaluate the $^3_\Lambda$H, $^4_\Lambda$He and $^5_\Lambda$He separation energies using the SMS NN potential at order N^{4}LO$^+$ and 3NFs at order N^{2}LO (for all the available cutoffs of $\Lambda_N = 400, 450, 500, 550$ MeV), in combination with the SMS YN potentials at orders NLO and N^{2}LO with cutoff $\Lambda_Y = 550$ MeV. In addition, for convergence study, we also perform calculations using the NN interactions at lower orders for the cutoff $\Lambda_N = 450$ MeV and the YN interaction at LO. Information on the employed SMS NN poten-

Table 1 Parameters c_i, c_D and c_E of the 3N interaction adjusted in conjunction with different orders and cutoffs Λ_N of the NN interaction (see [32] for details)

Order	Λ_N	c_1	c_3	c_4	c_D	c_E
N^{2}LO	400	–0.74	–3.61	2.44	8.0069	–0.94276
N^{2}LO	450	–0.74	–3.61	2.44	2.4850	–0.52793
N^{2}LO	500	–0.74	–3.61	2.44	–1.6262	–0.062696
N^{2}LO	550	–0.74	–3.61	2.44	–6.6840	0.85320
N^{3}LO	400	–1.20	–4.43	2.67	3.9998	–0.45796
N^{3}LO	450	–1.20	–4.43	2.67	1.5281	–0.35397
N^{3}LO	500	–1.20	–4.43	2.67	–0.4344	–0.31055
N^{3}LO	550	–1.20	–4.43	2.67	–2.7685	–0.12613
N^{4}LO	400	–1.23	–4.65	3.28	3.1275	–0.44217
N^{4}LO	450	–1.23	–4.65	3.28	0.65260	–0.35275
N^{4}LO	500	–1.23	–4.65	3.28	–1.5794	–0.32025
N^{4}LO	550	–1.23	–4.65	3.28	–3.9867	–0.32235
N^{4}LO$^+$	400	–1.23	–4.65	3.28	3.3278	–0.45405
N^{4}LO$^+$	450	–1.23	–4.65	3.28	0.8918	–0.38595
N^{4}LO$^+$	500	–1.23	–4.65	3.28	–1.2788	–0.38214
N^{4}LO$^+$	550	–1.23	–4.65	3.28	–3.6257	–0.41022

Λ_N is given in MeV, c_i in [GeV^{-1}] and c_D/c_E are dimensionless

tials can be found in Ref. [19], while the SMS YN potentials are described in Ref. [26]. The 3NFs are identical to the ones used in [32,33]. For completeness, we summarize the parameters c_i, c_D and c_E in Table 1 (see Eq. (1) in [32] for the definition). The c_i values used in [19] were obtained in Ref. [34] from matching the results of a Roy-Steiner analysis of pion-nucleon scattering to chiral perturbation theory. For the 3NFs at N^{3,4}LO, these values need to be shifted as outlined in [35] which is already taken into account in Table 1. The c_d and c_e LECs are fitted to the ^{3}H binding energy and the proton-deuteron differential cross-section minimum at the beam energy of $E_N = 70$ MeV [32].

Since we will compare to some results from Gazda et al. [22], the construction and the properties of the potential set NNLO$_{sim}$ used in [22] will be of relevance for the discussion below. The interactions are described in Ref. [27]. There, six different fitting regions for NN (namely $T_{lab} = 125, 158, 191, 224, 257, 290$ MeV, and seven cutoffs $\Lambda_N = 450, 475, \dots, 600$ MeV are considered. The LECs of these interactions are optimized by requiring a simultaneous description of NN as well as πN scattering cross sections, and binding energies and charge radii of the deuteron, ^{3}H, and ^{3}He. The combined analysis leads to πN LECs that are marginally consistent with the ones from the Roy-Steiner analysis and with much larger uncertainties [34]. Thus, it is preferable to use such knowledge directly as done e.g. in Ref. [19].

The strategy followed in the construction of the SMS NN potentials [19] that are employed in our investigation

is however different, cf. Sections 6.3 and 7.5.4 of that reference for a detailed discussion. Here a smaller (larger) energy range was considered for establishing the lower (higher) order NN potentials, which is in line with the expected pertinent validity range of the chiral expansion. Specifically, at N^{2}LO, N^{3}LO and N^{4}LO$^+$ NN data up to 125, 200 and 260 MeV, respectively, were fitted. The χ^2 obtained in the fit for different orders and different energy regions are listed in Table 3 of [19] for the cutoff $\Lambda_N = 450$ MeV. With that cutoff the overall best description of the NN data is achieved. Corresponding results for all cutoffs can be found in [36] (Table 6.9). One can see that for the N^{4}LO$^+$ potentials the χ^2/datum is excellent (close to 1) and practically independent of the cutoff, while for N^{2}LO the quality is rather different for the different energy regions and depends strongly on the cutoff. Clearly, the NN data at high energy cannot be well described by the NN interactions at low order. To the best of our knowledge, there is no detailed information on the χ^2 for the individual potentials of the set NNLO$_{sim}$. Finally, note that the NNLO$_{sim}$ potentials are based on a nonlocal regulator throughout while in the SMS NN potentials a local regulator is employed for the pion-exchange contributions. Here the range of optimal cutoffs is $400 - 550$ MeV [19], as already indicated above.

3 Uncertainties from the method

In the NCSM calculations, all potentials are evolved by a similarity renormalization group (SRG) transformation based on a flow parameter of $\lambda = 1.88$ fm^{-1} unless stated otherwise, see Refs. [31,37] for the technical details. SRG-induced YNN forces are taken into account (and, of course, both SRG-induced and chiral $3N$ forces) but no chiral YNN three-body forces ($3BF$s). In this section, we will discuss the uncertainties of our numerical approaches and quantify the effect of neglecting the SRG-induced four- and higher-body forces on the Λ separation energies B_Λ by carefully studying the dependence of the B_Λ's on the SRG-flow parameters. Note that results for the $A = 3(4)$ hypernuclei have been mainly obtained by solving a set of the FY equations, which are formed by rewriting the corresponding non-relativistic momentum-space Schrödinger equations, with the bare NN, $3N$ and YN interactions. The FY method is more efficient for light systems and has been very successfully applied to study both nuclei and hypernuclei up to four baryons [9–11,38]. In addition, it has also been carefully checked that the FY equations converge within less than 1(20) keV for $A = 3(4)$ hypernuclei, respectively (see also [11,18]). Hence, a direct comparison between the J-NCSM and the FY results for $^4_\Lambda$He will provide the most accurate estimate for the size of the neglected contributions from the induced higher-body forces in this system. Finally, the FY approach, in principle, could also be extended to $^5_\Lambda$He, however, the computation is rather challenging, therefore, for that system, we will only employ the J-NCSM. For details of the method and its implementation, we refer the reader to [16,17,31].

3.1 ω- and $\mathcal{N}_{\max}$-space extrapolation

As mentioned earlier, we will employ the J-NCSM to calculate the binding energies of systems with $A \geq 4$. This method is of course also applicable to $^3_\Lambda$H, however, because of its extremely small separation energy, the J-NCSM calculations for that system inhere an uncertainty that is significantly larger than the value of 1 keV for the Faddeev method. In general, the J-NCSM approach relies on an expansion of the many-body wavefunction in harmonic oscillator (HO) basis depending on relative Jacobi coordinates of all the particles involved. Such basis functions are characterized by the HO frequency ω and the total HO energy quantum number $\mathcal{N}$. In order to get a finite number of basis states for practical calculations, $\mathcal{N}$ is constrained by the model space size $\mathcal{N}_{\max}$ [16,31]. In practice, we perform the J-NCSM calculations for different sets of all the accessible model spaces up to $\mathcal{N}_{\max}$ and for a certain range of HO frequencies (which are close to the variational minimum at $\mathcal{N}_{\max}$). The converged binding energies are then obtained by performing an additional extrapolation to infinite model space. Several strategies have

been pursued to perform such extrapolations. Very often, an empirical exponential extrapolation in $\mathcal{N}_{\max}$ at a fixed HO frequency ω (usually the ones that yield the lowest binding energy for the largest computationally accessible model spaces) is employed [33,39–41]. In our works in [16,17,31] and also for this work, we pursue a slightly different strategy, namely a two-step extrapolation procedure. Here the first step is to minimize (eliminate) the HO-ω dependence of the binding energies $E(\omega, \mathcal{N}_{\max})$ utilizing the following (empirical) ansatz,

$$E(\omega, \mathcal{N}_{\max}) = E_{\mathcal{N}_{\max}} + \kappa(\log(\omega) - \log(\omega_{opt}))^2, \tag{1}$$

with $E_{\mathcal{N}_{\max}}$, ω_{opt} and κ being fitting parameters. The obtained lowest energies $E_{\mathcal{N}_{\max}}$ for each accessible $\mathcal{N}_{\max}$ are then used for the extrapolation to infinite model space assuming an exponential ansatz,

$$E_{\mathcal{N}_{\max}} = E_\infty + A e^{-B\mathcal{N}_{\max}}. \tag{2}$$

The final uncertainty is assigned as the difference between the infinite-model space extrapolated energy E_∞ and the one computed for the largest computationally accessible model space. The described two-step extrapolation procedure is applied to all nuclear and hypernuclear calculations of the present work. As for demonstration, we show in Fig. 1 the extrapolation for the ^{4}He binding energies that have been computed using the SMS N^{2}LO(550) NN potential. Here, we obtain a binding energy of $E(^4$He$) = -25.14 \pm 0.06$ MeV which is in a good agreement with the value of $E(^4$He$) = -25.15 \pm 0.02$ MeV that resulted from solving the FY equations. Clearly, our way of assigning the numerical uncertainty seems to be rather conservative, and a somewhat less conservative (but also empirical) estimate has been considered for example in [33,39–41]. Nevertheless, as one will see in the following section, using the SRG-evolved interactions, our NCSM results for $A = 4, 5$ hypernuclei converge almost perfectly (within several keV).

3.2 Infrared (IR) extrapolation

Let us further note that a truncation in the ω and $\mathcal{N}_{\max}$ model spaces also implies a finite infrared (IR) length scale, (L_{IR}), and an ultraviolet (UV) cutoff, Λ_{UV}, [41–44]. Hence, by recasting the binding energies $E(\omega, \mathcal{N}_{\max})$ in terms of L_{IR} and Λ_{UV}, $E(L_{IR}, \Lambda_{UV})$, one can also perform the infinite basis extrapolation with respect to the L_{IR} and Λ_{UV} cutoffs [41–44]. In general, the IR length scale (and Λ_{UV}) depends on the system considered and on how the basis functions are truncated. In the case of the NCSM with a total energy truncation a precise value for L_{IR} has been derived in [45]. Furthermore, it has also been shown that, at a sufficiently large and fixed Λ_{UV}, the leading order IR correction to the
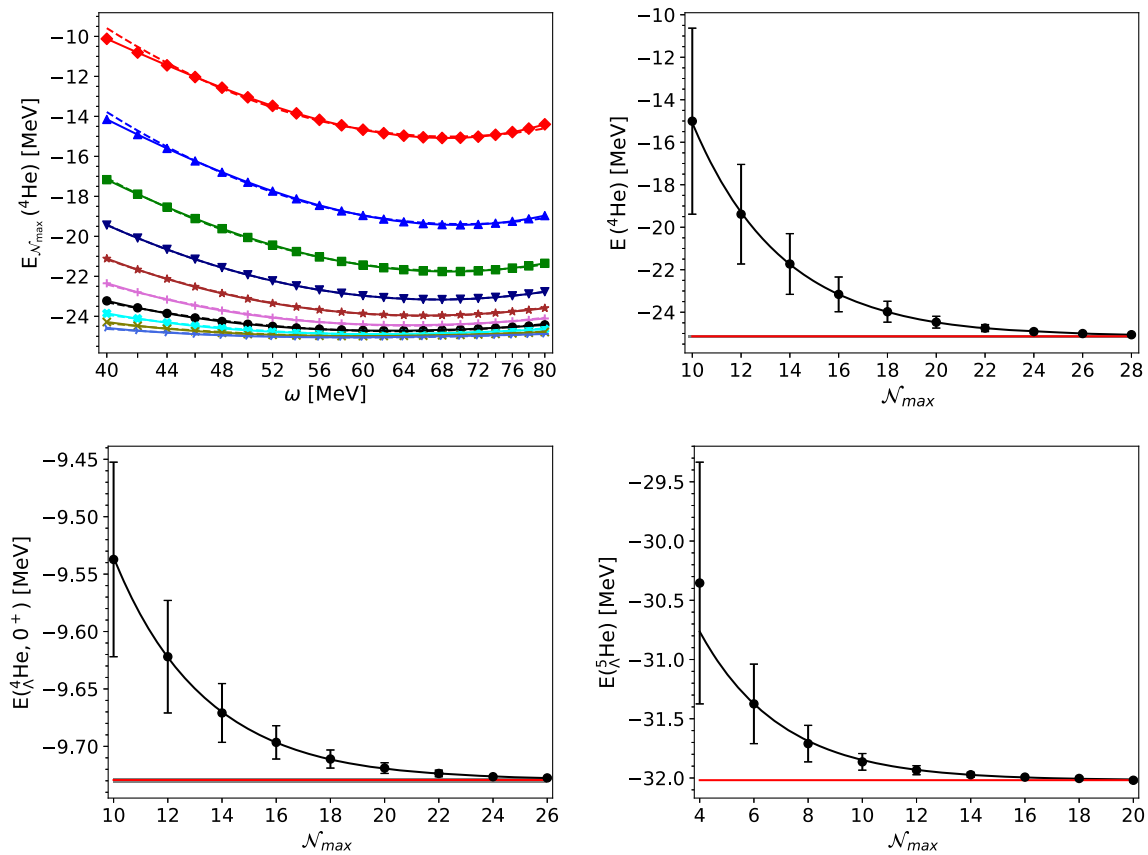
Fig. 1 Upper panel: two-step extrapolation procedure for $E(^4\text{He})$. ω-space extrapolation (left). The solid lines are the ^4He binding energies computed for different $\mathcal{N}_{max}$ from 10 to 28 with a step of 2. The dashed lines are obtained by using the ansatz Eq. (1). $\mathcal{N}_{max}$-space extrapolation (right). The horizontal line with shaded area shows the extrap-
olated binding energy and the estimated numerical uncertainty. The calculations are based on the SMS $\text{N}^2\text{LO}(550)$ NN potential. Lower panel: $\mathcal{N}$-space extrapolation for $E(^4_\Lambda\text{He})$ (left) and $E(^5_\Lambda\text{He})$ (right). The calculations are based on the SMS $\text{N}^4\text{LO}^+(450)$ NN potential with $\text{N}^2\text{LO}(450)$ $3N$ force, and the $\text{N}^2\text{LO}(550)$ YN potential

binding energy follows an exponential dependence on L_{IR} [41,45,46],

$$E_{\Lambda_{UV}}(L_{IR}) = E_{\Lambda_{UV},\infty} + a_{\Lambda_{UV}} e^{-2\kappa_{\Lambda_{UV},\infty} L_{IR}}. \qquad (3)$$

The UV correction is in general sensitive to the details of the employed interaction or, more precisely, on how the interaction is regularized [44]. This correction is not yet well understood in contrast to the IR energy correction. Hence, in practice, one often performs the IR extrapolation at a sufficiently large and fixed UV cutoff which yields reliable IR extrapolations and for which the UV error is approximately minimized (or suppressed) [22,47]. As an example, we show in Fig. 2 the IR extrapolated binding energy of ^4He, $E_{\Lambda_{UV},\infty}(^4\text{He})$, as a function of Λ_{UV}. The red triangles and blue circles are the binding energies computed using the SMS $\text{N}^2\text{LO}(550)$ and Idaho-$\text{N}^3\text{LO}(500)$ NN potentials, respectively. It clearly sticks out that, with the Idaho-$\text{N}^3\text{LO}(500)$ interaction (i.e. the one with a non-local regulator), the IR extrapolated results are practically stable for a sufficiently

large UV cutoff ($\Lambda_{UV} \geq 1300$ MeV). Indeed, the overall variation of $E_{\Lambda_{UV},\infty}(^4\text{He})$ for a range of UV cutoffs of $1300 \leq \Lambda_{UV} \leq 2100$ MeV is about 1 keV only. In contrast, for the $\text{N}^2\text{LO}(550)$ potential with a semi-local regulator, we observed a variation of about 90 keV even for very large Λ_{UV} but in a significantly smaller range, namely $1800 \leq \Lambda_{UV} \leq 2100$ MeV (see also the insert plot in Fig. 2). Evidently, the UV correction for the SMS interactions seems to be sizable and therefore should be carefully studied when the IR extrapolation is being used.

Finally, we have also adopted a Bayesian approach for the IR extrapolation as recently employed by Gazda et al. [22]. Here, we observed that the extrapolated results are rather sensitive to the hyperparameter chosen for $\Delta E_{\text{IR,max}}$, see Eqs. (28, 29) in [22]. By choosing $\Delta E_{\text{IR,max}}$ to be twice of the maximum extrapolation distance, we obtained the ^4He binding energies of $E(^4\text{He}) = -25.06 \pm 0.04$ and -25.12 ± 0.04 MeV for the $\text{N}^2\text{LO}(550)$ interaction at very large UV cutoffs of $\Lambda_{UV} = 1800$ and 2000 MeV, respec-
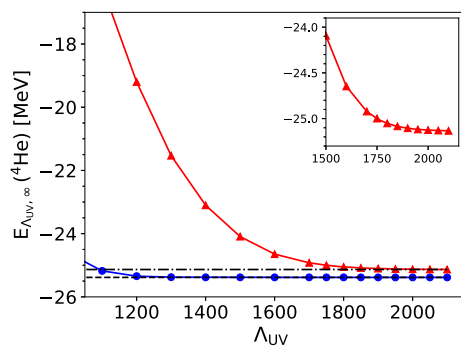
Fig. 2 IR extrapolation based on Eq. (3) of $E(^4\text{He})$ at different UV cutoffs Λ_{UV}. The calculations are based on the SMS N^{2}LO(550) (red triangles) and Idaho-N^{3}LO(500) (blue circles) NN potentials. Dash-dotted and dashed lines are the corresponding binding energies obtained using the extrapolation formula in Eq. (1)

Table 2 Λ separation energies $B_\Lambda(^4_\Lambda\text{He}, 0^+)$ and $B_\Lambda(^5_\Lambda\text{He})$ in MeV computed for different SRG flow parameters λ

| λ [fm^{-1}] | $B_\Lambda(^4_\Lambda\text{He}, 0^+)$ | | $B_\Lambda(^5_\Lambda\text{He})$ |
	N^{2}LO(550)	NLO(550)	N^{2}LO(550)
1.88	1.992 ± 0.002	2.061 ± 0.001	3.712 ± 0.001
2.00	1.991 ± 0.005	–	3.70 ± 0.005
2.236	1.990 ± 0.007	2.06 ± 0.006	3.708 ± 0.006
2.60	1.989 ± 0.014	2.06 ± 0.012	3.744 ± 0.008
3.00	1.985 ± 0.024	2.058 ± 0.023	3.806 ± 0.028
4.00	–	2.052 ± 0.021	–
∞	2.01 ± 0.02	2.08 ± 0.02	–

All calculations are based on the SMS NN potential N^{4}LO$^+$(450) and the $3N$ force at N^{2}LO(450). The SRG-induced $3N$ and YNN forces are also included. $B_\Lambda(^4_\Lambda\text{He}, 0^+)$ at $\lambda = \infty$ is obtained by solving the FY equations employing the bare NN, $3N$ and YN potentials. Note that $B_\Lambda(^4_\Lambda\text{He}, 0^+)$ at $\lambda = 4.0$ (3.0) fm^{-1} has been computed for model spaces up to $\mathcal{N}_{\max} = 34$ (28), respectively, whereas values at lower λ are computed for $\mathcal{N}_{\max} = 26$

tively. One sees that the latter energy is in a good agreement with the value of $E(^4\text{He}) = -25.14 \pm 0.06$ MeV that resulted from the two-step ω- and $\mathcal{N}_{\max}$ extrapolation and with the binding energy of $E(^4\text{He}) = -25.15 \pm 0.02$ obtained by solving the FY equations. Still, there is a non-negligible discrepancy of 60 keV between the two IR extrapolated results at $\Lambda_{UV} = 1800$ and 2000 MeV which could be attributed to the UV truncation or the high-order IR corrections. As discussed above, the latter is sensitive to the underlying interactions and their regulator and seems to be particularly significant for the SMS interactions. With the SRG-evolved potentials, the dependence on the chosen UV cutoff is somewhat reduced but it remains visible. In the following, we will therefore employ the two-step extrapolation to extract the final binding energies for $A = 4, 5$ systems. This extrapolation procedure is robust and it depends neither on the systems investigated nor on the underlying interactions. Let us finally stress that due to the SRG evolution and the very large model spaces employed in the calculations, our computed energies for $A = 4, 5$ hypernuclei at the largest model spaces practically converge. The final results should therefore not depend on the extrapolations.

3.3 Similarity Renormalization Group (SRG) for $^4_\Lambda\text{He}$, $^5_\Lambda\text{He}$

In order to study the different extrapolation methods, we have employed so far only the bare two-body NN interactions and provided examples for the ^4He system. There, one can clearly see that the NCSM calculations converge nicely even when the bare chiral NN interaction is employed. Note that $3N$ forces have been omitted in such calculations in order to save computational resources, but we do not expect that these change the convergence of the NCSM calculations significantly. However, when a hyperon is added to the $A = 3$ (4) nuclear systems, the NCSM calculations for $^4_\Lambda\text{He}$ ($^5_\Lambda\text{He}$) with the bare chiral SMS NN, $3N$ and YN interac-

tions do not converge well even when the largest computationally accessible model space, namely $\mathcal{N}_{\max} = 34$ (20), is employed. Not well-converged hypernuclear binding energies may impact the final conclusion about the nuclear model uncertainty in those hypernuclei. Therefore, to speed up the convergence of the NCSM calculations, we will evolve all the employed NN, $3N$ and YN potentials with an SRG transformation [23,37,48–50]. Like in our previous work [37], here both SRG-induced $3N$ and YNN forces are explicitly taken into account, while the SRG-induced four- and higher-body forces, whose contributions to the binding energies are expected to be small, are omitted. In most of the calculations below, we will use an SRG flow parameter of $\lambda = 1.88$ fm^{-1} which is widely employed in both nuclear [25,33,51,52] and hypernuclear calculations [23,37]. At that flow parameter, a numerical uncertainty of a few keV can be achieved for both $^4_\Lambda\text{He}$ and $^5_\Lambda\text{He}$ for the model space $\mathcal{N}_{\max} = 26$ and 18, respectively, see Fig. 1 (lower panels) and also Table 2. It is therefore not necessary to perform the calculations for the $A = 4, 5$ hypernuclei using our largest computationally accessible model spaces, namely $\mathcal{N}_{\max} = 34$ and 20, respectively.

Since we do not include any SRG-induced interactions beyond $3BF$s in the current study, it is essential to quantify the size of the possible contributions from those missing forces to the separation energies in the $A = 4, 5$ hypernuclei. For that purpose, we perform calculations for $B_\Lambda(^4_\Lambda\text{He}(0^+))$ and $B_\Lambda(^5_\Lambda\text{He})$ for a wide range of SRG flow parameters, namely $1.88 \leq \lambda \leq 3.0$ (4.0) fm^{-1}. The results are tabulated in Table 2. Note that the separation energy $B_\Lambda(^4_\Lambda\text{He}(0^+))$ at $\lambda = \infty$ (i.e. non SRG-evolved) has been computed by solving the FY equations with the bare NN, $3N$ and YN potentials. Overall, one observes a negligible variation in

Table 3 Separation energies (in MeV) for $^3_\Lambda$H, $^4_\Lambda$He, and $^5_\Lambda$He based on the N^{4}LO$^+$ *NN* potential with cutoffs $400-550$ MeV and with inclusion of the chiral 3*N* force at N^{2}LO

Λ_N [MeV]	$B_\Lambda(^3_\Lambda H)$ FY	$B_\Lambda(^4_\Lambda He, 0^+)$ NCSM	FY	$B_\Lambda(^4_\Lambda He, 1^+)$ NCSM	FY	$B_\Lambda(^5_\Lambda He)$ NCSM
500 (N^{2}LO)	0.118 ± 0.001	2.061 ± 0.002	2.06 ± 0.02	1.119 ± 0.009	1.12 ± 0.02	3.409 ± 0.007
450 (N^{2}LO)	0.125 ± 0.001	2.119 ± 0.002	2.13 ± 0.02	1.141 ± 0.007	1.16 ± 0.02	3.518 ± 0.008
450 (N^{3}LO)	0.122 ± 0.001	2.042 ± 0.002	2.07 ± 0.02	1.07 ± 0.009	1.09 ± 0.02	3.287 ± 0.008
400	0.127 ± 0.001	2.084 ± 0.002	2.12 ± 0.02	1.08 ± 0.009	1.10 ± 0.02	3.308 ± 0.008
450	0.123 ± 0.001	2.061 ± 0.001	2.08 ± 0.02	1.087 ± 0.009	1.10 ± 0.02	3.334 ± 0.008
500	0.118 ± 0.001	2.02 ± 0.001	2.03 ± 0.02	1.08 ± 0.009	1.09 ± 0.02	3.310 ± 0.008
550	0.113 ± 0.001	1.972 ± 0.001	1.96 ± 0.02	1.064 ± 0.009	1.07 ± 0.02	3.245 ± 0.009
Experiment [20]	0.164 ± 0.043	2.169 ± 0.042	($^4_\Lambda$H)	1.081 ± 0.046	($^4_\Lambda$H)	3.102 ± 0.030
		2.347 ± 0.036	($^4_\Lambda$He)	0.942 ± 0.036	($^4_\Lambda$He)	

For the interaction in the *YN* system the potential SMS NLO(550) is employed. Selected results for N^{2}LO and N^{3}LO *NN* potentials are included too

$B_\Lambda(^4_\Lambda He)$ (of about 10 ± 25 keV) over the considered range of the SRG parameter which strongly indicates that the omitted SRG-induced forces contribute insignificantly to $B_\Lambda(^4_\Lambda He)$. In addition, there is a negligibly small difference of about 25 ± 30 keV between the separation energies at $\lambda = \infty$ and at a finite flow parameter ($\lambda = 3.00$ fm^{-1}) consistent with zero within the numerical accuracy which again confirms the smallness of the possible correction from the missing induced higher-body forces to $B_\Lambda(^4_\Lambda He(0^+))$. We note that similarly small discrepancies (about 20 ± 20 keV) are also observed for the excited state separation energies $^4_\Lambda He(1^+)$, see Table 3. For the $^5_\Lambda He$ system, we do not have the result at $\lambda = \infty$, nevertheless, with the available results, one can still estimate a small contribution of about 100 ± 30 keV from the neglected SRG-induced forces. We will see below that this inaccuracy is significantly less than the uncertainty due to the truncation of the chiral expansion. Hence, both our numerical uncertainties and the truncated errors of the SRG evolution are sufficiently small which in turn will allow for an accurate estimate of the theoretical uncertainties due to the underlying interactions considered in the following section.

4 Uncertainties from the *NN* and *YN* interactions

Recently performed estimates for the truncation error of the chiral expansion for the nucleonic sector build primarily on approaches that do not rely on cutoff variations [19,25,28,30,33,53]. The cutoff dependence, or generally speaking the residual regulator dependence, does provide a measure for the effects of high-order contributions but it is not a reliable tool for estimating the theoretical uncertainty due to cutoff artifacts, see also the arguments in Sect. 7 of Ref. [28]. Thus, in order to investigate the convergence pattern of the separation energies of the considered hypernuclei

with increasing order, we have implemented the Bayesian approach of Refs. [30,54] and summarized in Appendix 1 of Ref. [55].

The calculations presented in this section utilize *NN* potentials from LO up to N^{4}LO$^+$ and include the leading 3*NF*s starting from N^{2}LO. However, they are without the leading chiral *YNN* interactions and, therefore, incomplete starting from order N^{2}LO. We refrain from using so-called "projected results" (see [56]) which assume experimental values for certain binding energies arguing that these results can be fitted once LECs of the missing terms have been adjusted. We will discuss below how the missing terms might alter uncertainty estimates.

4.1 Discussion of the variations

Let us first inspect the variation of the separation energies with the employed *NN* potentials. As already mentioned in the introduction, previous bound-state calculations by us suggested that the Λ separation energies of light hypernuclei are not very sensitive to the employed *NN* interaction [11,18]. For example, the variation of the separation energy for the SMS *NN* potential of Ref. [19] at order N^{4}LO$^+$ with cutoffs $\Lambda_N = 400-550$ MeV were found to be around 100 keV for $^4_\Lambda He/^4_\Lambda H$ [18]. Those for the hypertriton were in the order of only 10 keV. Variations of similar magnitude have been observed in earlier calculations based on phenomenological interactions [11].

Separation energies for $A = 3-5$ Λ hypernuclei, obtained within the NCSM approach and from solving FY equations, are summarized in Table 3. The calculations are based on the *NN* and 3*N* potentials at N^{4}LO$^+$ and N^{2}LO, respectively, with four different cutoffs. To describe the *YN* interaction the SMS NLO(550) potential has been employed. We consider also *NN* potentials up to N^{2}LO and N^{3}LO with selected
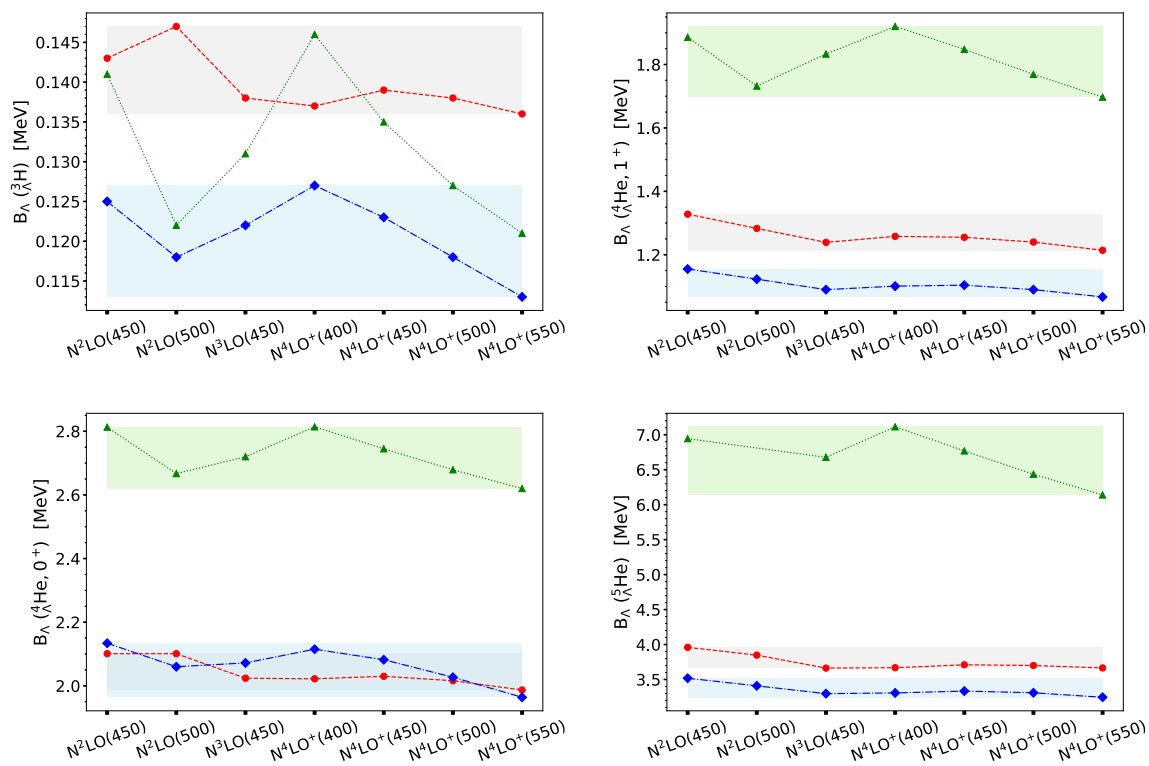
Fig. 3 Separation energies for $^3_\Lambda$H, $^4_\Lambda$He $(0^+, 1^+)$, and $^5_\Lambda$He, for different combinations of *NN* and *YN* interactions. *YN*: LO(600) (green triangles), SMS NLO(550) (blue diamonds), and SMS N^{2}LO(550) (red circles). 3*NF*s are included starting from N^{2}LO. The employed *NN*

interactions are specified on the x-axis. Shaded areas show the overall variation of the separation energies for the employed *YN* potentials at the given order. The band for LO in $^3_\Lambda$H was omitted since it covers 3/4 of the plot and obscures the size of the other bands

cutoffs for illustration. As already discussed above, the small deviations between the NCSM and FY results are due to SRG induced four-baryon interactions that are omitted in the calculations. It sticks out that the numerical uncertainty of the FY results is similar or even larger than the deviation to the NCSM results. Therefore, below we will estimate our uncertainties based on the NCSM results if available. A graphical representation of the separation energies is provided in Fig. 3. Here, in addition, results for the SMS N^{2}LO(550) *YN* potential as well as some results for the LO(600) *YN* potential are shown.

One can see from Table 3 that the overall variation of the $^5_\Lambda$He separation energy is indeed very small. Furthermore, in general, the variations are smaller than the difference to the experimental value. The latter difference will eventually be accounted for via inclusion of *YNN* 3*BF*s and/or with improved *YN* interactions. The situation for the $^4_\Lambda$He separation energies is similar. Also here for the 0^+ as well as for the 1^+ state, the variations due to the employed *NN* potential are small and specifically smaller than the difference to the empirical separation energies. Note that, since we do not include charge symmetry breaking potentials in the current study, our results for $B_\Lambda(^4_\Lambda\text{He})$ should be compared to the experimental values for both $^4_\Lambda$He and $^4_\Lambda$H hypernuclei.

A detailed overview of the variation of the separation energies for the considered hypernuclei due to different chiral orders and different cutoffs Λ_N of the underlying *NN* potentials is provided in Table 4, see also Fig. 3. For the set of N^{4}LO$^+$ *NN* potentials combined with the NLO or N^{2}LO *YN* interactions the variations of $B_\Lambda(^5_\Lambda\text{He})$ are $45 - 90$ keV. They increase to 295 keV when *NN* potentials of lower order are considered additionally. With regard to B_Λ of the $^4_\Lambda$He 1^+ state, the variation for the N^{4}LO set is only of the order of $25 - 44$ keV and increases to 114 keV when N^{2}LO/N^{3}LO *NN* interactions are taken into account. Concerning the 0^+ state, the variation for the N^{4}LO$^+$ set is $43 - 110$ keV. It becomes slightly larger but remains of similar magnitude by considering lower order *NN* interactions. Clearly, using the most sophisticated (and most accurate) *NN* interactions significantly reduces the sensitivity of B_Λ to the employed *NN* potentials. In passing, let us also mention that, as shown in Ref. [25], by including the higher-order corrections to the *NN* potentials up through fifth order, the systematic overbinding observed in nuclei with $A > 10$ reported in their earlier study in Ref. [32] when only *NN* and 3*N* interactions at N^{2}LO were employed, is practically resolved.

In order to compare the variations found by us with the ones reported by Gazda et al., we simply digitized their results

Table 4 Variation (ΔB_Λ) of $A = 3 - 5$ separation energies for SMS N^{4}LO$^+$ NN and N^{2}LO $3N$ potentials with cutoffs $400 - 550$ MeV and YN potentials of LO, NLO, and N^{2}LO (in keV)

	Considered $NN + YN$ potentials	$\Delta B_\Lambda(^3_\Lambda\text{H})$	$\Delta B_\Lambda(^4_\Lambda\text{He}, 0^+)$	$\Delta B_\Lambda(^4_\Lambda\text{He}, 1^+)$	$\Delta B_\Lambda(^5_\Lambda\text{He})$
NCSM/FY	N^{4}LO$^+$+N^{2}LO(550)	3	43	44	45
	N^{4}LO$^+$+NLO(550)	14	110	25	90
	N^{4}LO$^+$+LO(600)	25	194	223	970
	(N^{2}LO,N^{3}LO,N^{4}LO$^+$)+N^{2}LO(550)	11	114	114	295
	(N^{2}LO,N^{3}LO,N^{4}LO$^+$)+NLO(550)	14	147	88	273
FY [18]	N^{4}LO$^+$+NLO19(650)	10	85	50	
Refs. [21,22]	Variation with cutoff	50	270	240	1150
Ref. [22]	Standard deviation σ_{model}	20	100	100	400

(N^{2}LO,N^{3}LO, N^{4}LO$^+$) means that results for N^{2}LO and N^{3}LO NN potentials for selected cutoffs are considered, too

from Figs. 3 and 7 of Refs. [21,22], respectively. The corresponding values are also listed in Table 4. Actually, those authors considered variations due to the cutoff as well as variations due to the fitting region. The values we provide in the table are an average over those for different fitting regions. Obviously, the variations observed in that study are about 3 times larger for $^4_\Lambda$He (0^+), and practically a factor 10 larger for $^4_\Lambda$He (1^+) and $^5_\Lambda$He than the variations we find for the NLO and N^{2}LO YN potentials in combination with N^{4}LO$^+$ NN potentials. The variation for $B_\Lambda(^3_\Lambda\text{H})$ is likewise a factor 3 larger than ours. However, when we use a LO YN potential (see the corresponding line in Table 4 and Fig. 3) the variations become comparably large as those reported in [21,22].

We identified three possible sources for the differences in the variations. First, we expect a sensitivity to the actual size of the separation energies. In general, the LO YN interactions overbind the considered hypernuclei substantially (see Fig. 3 and also Tables I, II in [22]), and naturally, a significantly larger variation is expected. For $^3_\Lambda$H, the value of B_Λ is fixed by construction, for all considered YN potentials. Since here we observe an increased dependence on the NN interaction too, when a LO YN potential is used, we believe that the lack of short-range repulsion in the LO YN potentials is also a potential source for the difference to the results with NLO and N^{2}LO. This deficiency of the LO interactions can lead to an increased sensitivity to the details of the short-range part of the NN interactions. Third, there is presumably an effect from the employed regularization scheme. The N^{2}LO$_{sim}$ potentials employed by Gazda et al. build on a non-local regulator for all components of the interaction. The SMS NN potentials by Reinert et al. are based on a novel regularization scheme where a local regulator is applied to the pion-exchange contributions and only the contact terms, being non-local by themselves, are regularized with a non-local function. As discussed thoroughly in [19,28], a local regulator for pion-exchange contributions leads to a reduc-

tion of the distortion in the long-range part of the interaction and, thereby, facilitates a more rapid convergence already at low chiral orders. This affects predominantly P- and higher partial waves. In this context note that the optimal cutoff range is shifted from $450 - 600$ MeV (Carlsson et al. [27]) to $400 - 550$ MeV (Reinert et al [19]).

Finally, and for clarification, we want to emphasize that the "model uncertainties" quoted in the abstract and in the summary of Ref. [22], have been deduced from the variance $\sigma^2(\text{NNLO}_{\text{sim}})$ as specified in Eq. (33) of that paper. As for reference those uncertainties are listed in the last line of Table 4. It is important to stress that those values, which are noticeably smaller than the variations, cannot and should not be compared with our results.

4.2 Estimate for the truncation error

Given that we have results for different orders of the chiral NN and YN interactions at our disposal, we are now able to perform a more complete analysis of the uncertainties due to truncation in the chiral expansion. To this aim, we follow the Bayesian approach of [54] and Ref. [55], cf. the appendix on the pointwise model. Assume that the observable X (here the separation energies) also follow the power counting of the potential. If the chiral expansion is truncated at order K, the observable X_K and the corresponding truncation error δX_K can be expressed as

$$X_K = X_{\text{ref}} \left(\sum_{k=0}^{K} c_k Q^k \right); \quad \delta X_K = X_{\text{ref}} \left(\sum_{k=K+1}^{\infty} c_k Q^k \right).$$
(4)

where $Q = M_\pi^{\text{eff}}/\Lambda_b$ is the chiral EFT expansion parameter [57], X_{ref} is a dimensionful quantity that sets the overall scale and c_k are the dimensionless expansion coefficients. The expansion parameter is given by an effective pion mass M_π^{eff} and the breakdown scale Λ_b. The expansion coeffi-
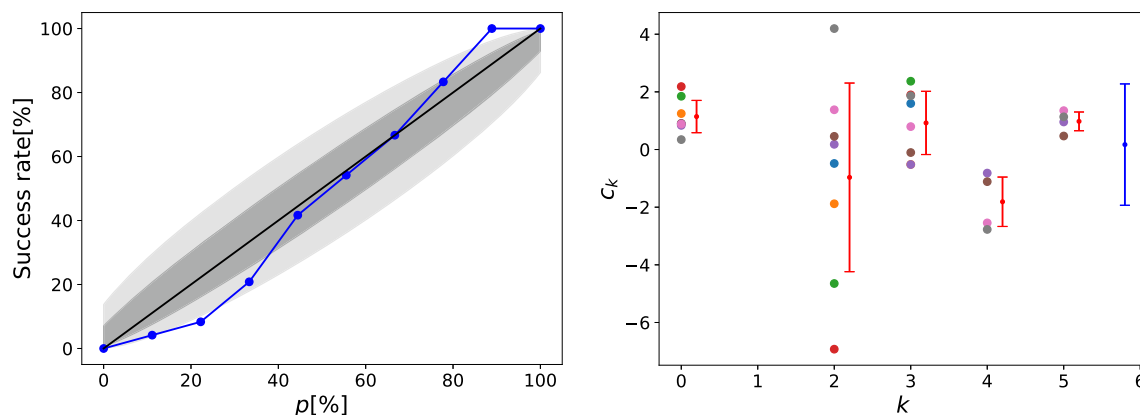
Fig. 4 (Left) Consistency plots for comparing the actual changes in higher orders to the expected values for $p[\%]$ DoB intervals. (Right) Values of the c_k coefficients extracted using the corresponding experi-

mental separation energies as the reference value. Also shown are the average and standard variation order by order and in total

cients c_k ($k = 0, 2, \cdots K$) are obtained from the separation energies computed at two consecutive orders, $c_{k+1} = (B_\Lambda^{(k+1)} - B_\Lambda^{(k)})/(Q^{k+1} X_{\text{ref}})$. In order to obtain the posterior probability distribution for the truncation error δX_K based on our knowledge of the coefficients c_k ($k = 0, 2, \cdots K$), we further assume that all the expansion coefficients are independently and identically distributed (iid). The priors follow the "pointwise" distribution given in Eq. (A2) in the appendix of Ref. [55], namely a normal distribution with variance $\bar{c}^2$

$$c_k | \bar{c}^2 \overset{\text{iid}}{\sim} \mathcal{N}(0, \bar{c}^2) \tag{5}$$

where the distribution of $\bar{c}^2$ follows an inverse χ^2 distribution

$$\bar{c}^2 \sim \chi^{-2}(\nu_0, \tau_0^2) \tag{6}$$

depending on the two hyperparameters ν_0 and τ_0^2. The analytical expression for the posterior distribution of the truncation error δX_K is also given in Eq. (A12) of the same appendix.

Clearly, the truncation error will be contingent on the expansion parameter Q as well as on our choices for the parameters ν_0 and τ_0^2. We have compared results for non-informative priors (not preferring any maximal value of c_k, i.e. using the parameter $\nu_0 = 0$) and more informative priors for c_k with $\nu_0 > 0$. It turns out that the estimated truncation errors were not very sensitive to this parameter, therefore, we finally chose $\nu_0 = 1.5$ which was also used in [25] for studying the convergence of calculations of ordinary nuclei. We also followed [25] and selected $\tau_0^2 = 2.25$.

To learn the expansion parameter Q, we assume a normal distribution for the prior of Q and use the expression in Eq. (A19) of Ref. [55] to compute the posterior distribution of Q. In order to increase the statistics, when learning the expansion parameter Q we employ the combined data that contains all the separation energies for $A = 3 - 5$ hypernuclei computed at different orders of NN and of YN interac-

tions. We obtained the value of $Q = 0.4$, which is slightly larger than the one used for ordinary nuclei [25]. This could probably be related to the small number of our data that are available for determining the distributions. We also test the validity of our choice for Q by generating consistency plots as proposed in Ref. [54] that show the comparison between the obtained rates of the overlap of higher-order calculations with lower-order degree of believe (DoB) intervals and the expected values, see Fig. 4. Clearly, with the chosen value of $Q = 0.4$, our uncertainty estimates are statistically consistent with the observed changes due to higher-order contributions. Finally, let us remark that we also extracted the Q parameter using two other sets of data, referring to as the NN and YN convergence studies. In the former case, the data are composed of separation energies at various NN orders ($k = 0, 2, 3, 4, 5$) but with a fixed YN order. In the latter case, we used the data set that consists of the energies at a fixed NN order but for different YN orders ($k = 0, 2, 3$). The obtained Q values in the two cases are in general consistent with each other and with the result obtained when the combined data is used. The most relevant difference between the NN and YN convergence studies was probably the fact that the expansion parameter Q tends to be smaller for NN than for YN. The deviation was, however, small enough so that a combined-data analysis is preferred because of its higher statistics. Therefore, we will use the expansion parameter $Q = 0.4$ for estimating the truncation errors.

The obtained distribution of c_k coefficients is also interesting. Their dependence on the order k of the expansion is shown on the right panel of Fig. 4 together with the average values per order and the complete average with standard deviation. For their extraction, we chose reference values close to the corresponding experimental separation energies in order to be independent of the LO result. The latter might be altered by choosing a quite small singlet scattering length in order

to match the $^3_\Lambda$H separation energy [58]. In addition, because of this choice for X_{ref}, we are able to use all coefficients for determining the posteriors. We stress that the final truncation errors are independent of the reference value. Interestingly, the NLO coefficients have a tendency to be larger than all the other ones. This tendency is also observed for the expansion coefficients obtained for light nuclei [25]. Overall, all the expansion coefficients are however of natural size and, therefore, the value of $Q = 0.4$ for the expansion scale seems to be consistently chosen. For this extraction, it has been assumed that the differences of the higher-order contributions are of the order naively expected. We have also attempted to analyse the results assuming that the expected corrections at N^{2}LO and at higher orders are of the order $k = 3$ because the chiral YNN forces contributing at this order is missing. In this case, the higher-order NN expansion coefficients become unnaturally small. This in turn supports our assumption that these differences are indeed of the expected order. Note that this assumption is however not true for the regulator dependence which will ultimately be counterbalanced by a YNN $3BF$ once it has been taken into account. The cutoff dependence is therefore a Q^3 effect for NLO and all higher orders.

Having the hyperparameters and the expansion scale fixed, we are now at the position to analyze the convergence pattern of the separation energies with respect to chiral order. As already documented in the previous section, the separation energies are much less sensitive to the NN than to the YN interaction. This is also manifest in a different size of c_k coefficients for the NN convergence and the YN convergence. We therefore analyze the convergence and extract the truncation uncertainties for NN and YN separately. The convergence of the separation energies for $A = 3 - 5$ hypernuclei with respect to NN and YN orders are shown in the left and right panels in Fig. 5, respectively. The bands show the expected truncation errors at each orders. Clearly, the large expansion parameter leads only to a slow decrease of this uncertainty at higher orders.

It clearly sticks out that the variation due to the NN interaction is much smaller than the one due to the YN interaction. In order to compare the NN cutoff variation with the relevant uncertainty estimate, we include also results for different NN cutoffs, see green points. Although these calculations were performed at order N^{4}LO$^+$, we show them in the figure at NLO since the cutoff variation will be ultimately mostly observed by the only N^{2}LO contribution that we are not taking into account, namely the leading YNN $3BF$. As can be seen, the NN cutoff variation is consistent with but in most of the case smaller than the 68% DoB interval. This is consistent with our observation in the previous section and with the general expectation that the cutoff variation as well as the dependence on the chiral order of the NN interaction is of less relevance when predicting Λ separation energies.

The most dominant uncertainty is due to the truncation of the chiral expansion of the YN interaction, as can be clearly seen in the right panel in Fig. 5. Here the grey bands indicate the uncertainty at NLO attached to the result at order N^{2}LO. This is the relevant quantity for the comparison to the experimental separation energies shown in red symbols since all calculations do not include the leading chiral YNN $3BF$. Note that both experimental separation energies of $^4_\Lambda$H and $^4_\Lambda$He are included in the figure because our calculations have been performed with isospin conserving interactions that cannot properly predict the charge symmetry breaking differences of the separation energies of these mirror hypernuclei. It can be seen that all experimental energies are within the 68% DoB intervals. The NLO uncertainties are substantial and significantly larger than the experimental uncertainties for $A = 4$ and 5. Only for $^3_\Lambda$H, the experimental and theoretical uncertainty are comparable, justifying our choice to constrain the strength of the YN interaction in the $^1S_0$ partial wave by the $^3_\Lambda$H separation energy [26,59].

In order to obtain an estimate of the size of the missing YNN force contributions, we have summarized half the size of the NLO 68% DoB interval in Table 5 for both, the NN and the YN convergence. The dependence on the NN interaction is generally a factor of two smaller than the one on the YN interaction. It is however larger than the one anticipated from older calculations comparing results for different phenomenological NN interactions [11]. Incidentally, the values are roughly in line with the "model uncertainties" from Ref. [22] that were based on averaging of the interactions dependence. As discussed in the previous subsection, the true dependence on the NN interaction is actually larger, c.f. Table 4.

The relevant quantity for assessing the size of the YNN $3BF$ is the NLO 68% DoB for YN since this quantity is larger. The $3BF$ contribution for the hypertriton is estimated to be roughly 15 keV. It is compatible with the result of a first explicit (though incomplete) evaluation of $3BF$s for $^3_\Lambda$H by Kamada et al. [60], which suggests a contribution of around 20 keV. In that work only the contribution due to 2π-exchange has been taken into account. We consider the nice agreement as a confirmation for the procedure we follow. In any case, it is important to note that the $3BF$ effect on the hypertriton separation energy is found/estimated to be smaller than the experimental uncertainty.

For $A = 4$, the YNN $3BF$ can be expected to contribute in the order of 200 keV. Also this estimate is in line with previous results. In Ref. [18], we observed that the NLO13 and NLO19 YN potentials exhibit a regulator dependence of up to 210 keV and variations of the separation energies of up to 320 keV due to dispersive effects associated with the ΛN-ΣN coupling which both can be taken as estimate for YNN $3BF$ contributions. The estimate here, based on the convergence pattern of the chiral expansion, is of similar

Fig. 5 Comparison of the convergence with respect to the chiral order of the employed *NN* (left) and *YN* (right) potentials for $^{3}_{\Lambda}$H, $^{4}_{\Lambda}$He(0$^+$), $^{4}_{\Lambda}$He(1$^+$) and $^{5}_{\Lambda}$He (from top to bottom)
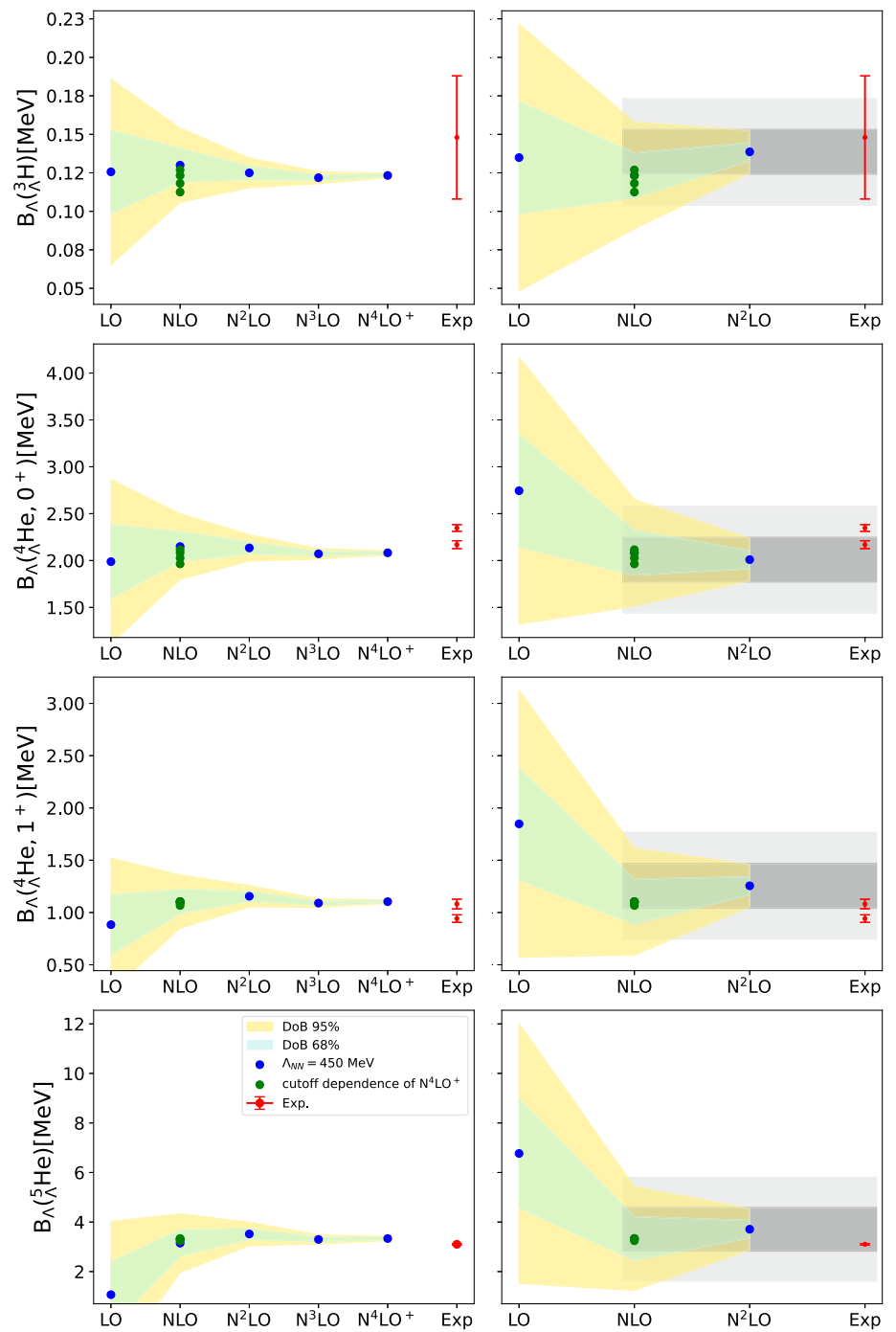

Table 5 Half the size of the 68% DoB intervals for the Λ separation energy at NLO based on the convergence with respect to the *YN* and *NN* interactions (in MeV)

Nucleus	$\Delta_{68}(NN)$	$\Delta_{68}(YN)$
$^{3}_{\Lambda}$H	0.01	0.02
$^{4}_{\Lambda}$He (0$^+$)	0.16	0.24
$^{4}_{\Lambda}$He (1$^+$)	0.11	0.21
$^{5}_{\Lambda}$He	0.53	0.88

size. For $^5_\Lambda$He, the comparison of NLO19 and NLO13 can again provide hints to the size of $3BF$ effects. We found in Ref. [37] that the result for NLO13 and NLO19 differs by 1.1 MeV which gives a lower bound of possible YNN-force contributions. Therefore, also the estimate in Table 5 of 900 keV appears to be reasonable.

Additionally, we employed the approach proposed by Epelbaum, Krebs and Meißner (EKM) [28] for estimating the uncertainty as outlined in the appendix. This estimated error depends strongly on the expansion parameter chosen. It turns out that for standard values of $Q = 0.31$, the estimates are well in line with the Bayesian results. For $Q = 0.4$, the EKM estimates are somewhat larger but still of similar order as the statistically motivated ones.

It is also interesting to look at the prospective N^2LO uncertainties once the leading YNN interactions are included. In our analysis, we find 6, 100 and 350 keV for the A=3, 4 and 5 hypernuclei, respectively. These estimates are however strongly dependent on the expansion parameter Q. For example, for $Q = 0.3$ as in [25], we find N^2LO uncertainties of 3, 50 and 200 keV.

5 Summary

In this work, we have investigated various aspects relevant for the theoretical uncertainties of calculations of separation energies of Λ hypernuclei with $A \leq 5$. These light hypernuclei have attracted some attention recently because their properties are mostly determined by the S-wave YN interactions which are reasonably well constrained by the available YN data and the hypertriton separation energy. To a great extent the effort for providing a quantitative assessment of the uncertainties of our few-body calculations was motivated by the study of Gazda et al. [22] which suggested that even the employed NN ($3N$) interactions might have an significant impact on the uncertainty of the predicted hyperon separation energies.

In the present work, we considered two possible sources for uncertainties. First, there is the numerical uncertainty which, in our case, is caused by discretization and/or truncation of the model space in the no-core shell model calculation, and also due to neglected contributions of SRG-induced four- and more-baryon interactions. By comparing two extrapolation methods and benchmarking to results from FY calculations, we found that the numerical uncertainties are well under control and are actually irrelevant in comparison to other effects. The other source of uncertainties considered are differences in the employed NN (plus $3N$) and YN potentials. Our results for the hyperon separation energies do show some dependence on the underlying NN interaction. However, compared to Gazda et al. [22], the variations are considerably smaller. A detailed analysis of our calculations suggests that the significant reduction is very likely

due to the use of higher order YN interactions and of higher order NN interactions. In fact, the effects due to truncating the chiral order of the YN interaction are the larger and most relevant ones and have been quantified in this work for the first time. It should be said that the way how regularization is implemented (all non-local or semi-local) could play a role, too, though on a less significant level.

Altogether, it is reassuring to observe that our NLO and (incomplete) N^2LO results agree with the experimental separation energies within the estimated NLO truncation error. They show that it is now of high importance to also include the missing chiral YNN three-body force that starts contributing at order N^2LO. Work in this direction is in progress. The present calculation indicates that their contribution is needed and can lead to a consistent and accurate description of all s-shell hypernuclei.

Independently, it is important to get more experimental input to facilitate a better determination of the YN interaction. Indeed, in the future more extensive data on the Λp system, i.e. angular distributions and possibly polarizations, should become available thanks to the J-PARC E86 experiment [61]. A major advantage of the 3N system is that there the underlying NN interaction can be examined also via Nd scattering and/or break-up observables. Some of the observables accessible in this way are known to be not very sensitive to the $3NF$ and, thus, provide an excellent direct and reliable testing ground for the properties of the NN potentials. Unfortunately, so far, for Λd scattering, we have neither data nor calculations based on modern YN interactions. However, there are plans for measurements of Λd scattering at JLab [62] and experimental studies of the Λd correlation function [63] are under way at CERN by the ALICE Collaboration [64]. Finally, also a Λnn resonance [65] would provide an important additional constraint, though its existence is still under debate.

Appendix A: Uncertainty estimate following EKM

For estimating the truncation error of the chiral expansion we also applied the EKM approach [28]. The concrete expression used to calculate an uncertainty δX^{NLO} to the NLO prediction X^{NLO} of a given observable X is [28,56]

$$\delta X^{\mathrm{NLO}}(Q) = \max\left(Q^3 \times \left| X^{\mathrm{LO}}(Q) \right|, \right.$$
$$\left. Q \times \left| X^{\mathrm{LO}}(Q) - X^{\mathrm{NLO}}(Q) \right| \right). \qquad \text{(A.1)}$$

We also note that the additional constraints specified in Eq. (8) of Ref. [56] are imposed. In Refs. [53,57], the expan-

Table 6 EKM uncertainty estimates in MeV at order NLO using different YN (1st and 2nd line) and NN (3rd and 4th line) orders for $^3_\Lambda$H, $^4_\Lambda$He, $^5_\Lambda$He for two values of the expansion parameter Q

Q	$^3_\Lambda$H	$^4_\Lambda$He(0^+)	$^4_\Lambda$He(1^+)	$^5_\Lambda$He
0.31	0.015	0.30	0.36	1.1
0.40	0.015	0.39	0.47	1.4
0.31	0.005	0.06	0.07	0.64
0.40	0.008	0.13	0.09	0.83

sion parameter Q was estimated to be $Q = 0.31$. This value was also used in nucleonic few-body studies [32,53]. We adopt here also the value of $Q = 0.4$ obtained in the Bayesian analysis, cf. Section 4.2. Using this ansatz to estimate the uncertainty, we obtain the results listed in Table 6 for the uncertainties due to the truncation.

In Ref. [54], it was found that the EKM uncertainty estimates correspond at NLO to the 68% DoB interval for a specific choice of the prior. Here, we find that the values are of similar order as the Bayesian analysis. Choosing the same expansion coefficient as in our Bayesian analysis, the actual values are somewhat larger. Only for the standard choice $Q = 0.31$, we find good agreement between the two uncertainty estimates.

References

1. G. Alexander et al., Study of the lambda-n system in low-energy lambda-p elastic scattering. Phys. Rev. **173**, 1452–1460 (1968)
2. B. Sechi-Zorn, B. Kehoe, J. Twitty, R.A. Burnstein, Low-energy lambda-proton elastic scattering. Phys. Rev. **175**, 1735–1740 (1968)
3. J.A. Kadyk, G. Alexander, J.H. Chan, P. Gaposchkin, G.H. Trilling, Lambda p interactions in momentum range 300 to 1500 mev/c. Nucl. Phys. B **27**, 13–22 (1971)
4. J.M. Hauptman, J.A. Kadyk, G.H. Trilling, Experimental Study of Lambda p and xi0 p Interactions in the Range 1-GeV/c-10-GeV/c. Nucl. Phys. B **125**, 29–51 (1977)
5. J. Rowley et al., Improved Λp Elastic Scattering Cross Sections Between 0.9 and 2.0 GeV/c and Connections to the Neutron Star Equation of State. Phys. Rev. Lett. **127**(27), 272303 (2021)
6. R.H. Dalitz, B.W. Downs, Hypernuclear binding energies and the Lambda-Nucleon interaction. Phys. Rev. **111**, 967–986 (1958)
7. J.J. de Swart, C. Dullemond, Effective range theory and the low energy hyperon-nucleon interactions. Ann. Phys. **19**(3), 458–495 (1962)
8. K. Dietrich, H.J. Mang, R. Folk, Binding energies of light hyperfragments. Nucl. Phys. **50**, 177–201 (1964)
9. K. Miyagawa, W. Glöckle, Hypertriton calculation with meson theoretical nucleon-nucleon and hyperon nucleon interactions. Phys. Rev. C **48**, 2576 (1993)
10. K. Miyagawa, H. Kamada, Walter Glöckle, V. G. J. Stoks, Properties of the bound Lambda (Sigma) N N system and hyperon nucleon interactions. Phys. Rev. C **51**, 2905 (1995)
11. A. Nogga, H. Kamada, W. Glöckle, The Hypernuclei $^4_\Lambda$He and $^4_\Lambda$He: challenges for modern hyperon nucleon forces. Phys. Rev. Lett. **88**, 172501 (2002)
12. R. Wirth, P. Gazda, D. Navrátil, A. Calci, J. Langhammer, R. Roth, Ab initio description of p-shell hypernuclei. Phys. Rev. Lett **113**(19), 192502 (2014)
13. R. Wirth, R. Roth, Induced hyperon-nucleon-nucleon interactions and the hyperon puzzle. Phys. Rev. Lett. **117**, 182501 (2016)
14. R. Wirth, D. Gazda, P. Navrátil, R. Roth, Hypernuclear no-core shell model. Phys. Rev. C **97**(6), 064315 (2018)
15. R. Wirth, R. Roth, Light neutron-rich hypernuclei from the importance-truncated no-core shell model. Phys. Lett. B **779**, 336–341 (2018)
16. S. Liebig, U.-G. Meißner, A. Nogga, Jacobi no-core shell model for p-shell nuclei. Eur. Phys. J. A **52**(4), 103 (2016)

17. H. Le, J. Haidenbauer, U.-G. Meißner, A. Nogga, Implications of an increased Λ-separation energy of the hypertriton. Phys. Lett. B **801**, 135189 (2020)
18. J. Haidenbauer, U.-G. Meißner, A. Nogga, Hyperon-nucleon interaction within chiral effective field theory revisited. Eur. Phys. J. A **56**(3), 91 (2020)
19. P. Reinert, H. Krebs, E. Epelbaum, Semilocal momentum-space regularized chiral two-nucleon potentials up to fifth order. Eur. Phys. J. A **54**(5), 86 (2018)
20. P. Eckert, P. Achenbach, et al. Chart of hypernuclides—Hypernuclear structure and decay data, 2021. https://hypernuclei.kph.uni-mainz.de
21. T.Y. Htun, D. Gazda, C. Forssén, Y. Yan, Systematic nuclear uncertainties in the hypertriton system. Few Body Syst. **62**(4), 94 (2021)
22. D. Gazda, T. Yadanar Htun, C. Forssén, Nuclear physics uncertainties in light hypernuclei. Phys. Rev. C **106**(5), 054001 (2022)
23. R. Wirth, R. Roth, Similarity renormalization group evolution of hypernuclear Hamiltonians. Phys. Rev. C **100**(4), 044313 (2019)
24. D.R. Entem, R. Machleidt, Y. Nosyk, High-quality two-nucleon potentials up to fifth order of the chiral expansion. Phys. Rev. C **96**(2), 024004 (2017)
25. P. Maris et al., Nuclear properties with semilocal momentum-space regularized chiral interactions beyond N2LO. Phys. Rev. C **106**(6), 064002 (2022)
26. J. Haidenbauer, U.-G. Meißner, A. Nogga, H. Le, Hyperon–nucleon interaction in chiral effective field theory at next-to-next-to-leading order. Eur. Phys. J. A **59**(3), 63 (2023)
27. B. D. Carlsson, A. Ekström, C. Forssén, D. Fahlin Strömberg, G. R. Jansen, O. Lilja, M. Lindby, B. A. Mattsson, K. A. Wendt, Uncertainty analysis and order-by-order optimization of chiral nuclear interactions. Phys. Rev. X **6**(1), 011019 (2016)
28. E. Epelbaum, H. Krebs, U.-G. Meißner, Improved chiral nucleon-nucleon potential up to next-to-next-to-next-to-leading order. Eur. Phys. J. A **51**(5), 53 (2015)
29. R.J. Furnstahl, D.R. Phillips, S. Wesolowski, A recipe for EFT uncertainty quantification in nuclear physics. J. Phys. G **42**(3), 034028 (2015)
30. R.J. Furnstahl, N. Klco, D.R. Phillips, S. Wesolowski, Quantifying truncation errors in effective field theory. Phys. Rev. C **92**(2), 024005 (2015)
31. H. Le, J. Haidenbauer, U.-G. Meißner, A. Nogga, Jacobi no-core shell model for p-shell hypernuclei. Eur. Phys. J. A **56**(12), 301 (2020)
32. P. Maris et al., Light nuclei with semilocal momentum-space regularized chiral interactions up to third order. Phys. Rev. C **103**(5), 054001 (2021)
33. P. Maris, H. Le, A. Nogga, R. Roth, J.P. Vary, Uncertainties in ab initio nuclear structure calculations with chiral interactions. Front. Phys. **11**, 1098262 (2023)
34. M. Hoferichter, J. Ruiz de Elvira, B. Kubis, U.-G. Meißner, Matching pion-nucleon Roy-Steiner equations to chiral perturbation theory. Phys. Rev. Lett. **115**(19), 192301 (2015)
35. V. Bernard, E. Epelbaum, H. Krebs, Ulf-G. Meißner, Subleading contributions to the chiral three-nucleon force. I. Long-range terms. Phys. Rev. C **77**, 064004 (2008)
36. P. Reinert. *Precision studies in the two-nucleon system using chiral effective field theory*. PhD thesis, Ruhr U., Bochum, 2022
37. H. Le, J. Haidenbauer, U.-G. Meißner, A. Nogga, Ab initio calculation of charge-symmetry breaking in A=7 and 8 Λ hypernuclei. Phys. Rev. C **107**(2), 024002 (2023)
38. A. Nogga. *Nuclear and hypernuclear three- and four-body bound states*. PhD thesis, Bochum University, 2001
39. P. Maris, J.P. Vary, A.M. Shirokov, Ab initio no-core full configuration calculations of light nuclei. Phys. Rev. C **79**, 014308 (2009)
40. E.D. Jurgenson, P. Maris, R.J. Furnstahl, P. Navratil, W.E. Ormand, J.P. Vary, Structure of p-shell nuclei using three-nucleon interactions evolved with the similarity renormalization group. Phys. Rev. C **87**(5), 054312 (2013)
41. Sidney A. Coon, Matthew I. Avetian, Michael K. G. Kruse, U. van Kolck, Pieter Maris, James P. Vary, Convergence properties of *ab initio calculations of light nuclei in a harmonic oscillator basis*. Phys. Rev. C **86**, 054002 (2012)
42. I. Stetcu, B.R. Barrett, U. van Kolck, No-core shell model in an effective-field-theory framework. Phys. Lett. B **653**, 358–362 (2007)
43. E.D. Jurgenson, P. Navrátil, R.J. Furnstahl, Evolving nuclear many-body forces with the similarity renormalization group. Phys. Rev. C **83**(3), 034301 (2011)
44. S. König, S.K. Bogner, R.J. Furnstahl, S.N. More, T. Papenbrock, Ultraviolet extrapolations in finite oscillator bases. Phys. Rev. C **90**, 064007 (2014)
45. K.A. Wendt, C. Forssén, T. Papenbrock, D. Sääf, Infrared length scale and extrapolations for the no-core shell model. Phys. Rev. C **91**(6), 061301 (2015)
46. R.J. Furnstahl, T. Papenbrock, S.N. More, Systematic expansion for infrared oscillator basis extrapolations. Phys. Rev. C **89**(4), 044301 (2014)
47. C. Forssén, B.D. Carlsson, H.T. Johansson, D. Sääf, A. Bansal, G. Hagen, T. Papenbrock, Large-scale exact diagonalizations reveal low-momentum scales of nuclei. Phys. Rev. C **97**(3), 034328 (2018)
48. S.K. Bogner, R.J. Furnstahl, R.J. Perry, Similarity renormalization group for nucleon–nucleon interactions. Phys. Rev. C **75**, 061001 (2007)
49. S.K. Bogner, R.J. Furnstahl, R.J. Perry, Three-body forces produced by a similarity renormalization group transformation in a simple model. Ann. Phys. **323**, 1478 (2008)
50. E.D. Jurgenson, P. Navrátil, R.J. Furnstahl, Evolution of nuclear many-body forces with the smilarity renormalization group. Phys. Rev. Lett. **103**(8), 082501 (2009)
51. P. Maris et al., Properties of 4He and 6Li with improved chiral EFT interactions. EPJ Web Conf. **113**, 04015 (2016)
52. S. Binder et al., Few-nucleon and many-nucleon systems with semilocal coordinate-space regularized chiral nucleon–nucleon forces. Phys. Rev. C **98**(1), 014002 (2018)
53. E. Epelbaum et al., Towards high-order calculations of three-nucleon scattering in chiral effective field theory. Eur. Phys. J. A **56**(3), 92 (2020)
54. J.A. Melendez, S. Wesolowski, R.J. Furnstahl, Bayesian truncation errors in chiral effective field theory: nucleon–nucleon observables. Phys. Rev. C **96**(2), 024003 (2017)
55. J.A. Melendez, R.J. Furnstahl, D.R. Phillips, M.T. Pratola, S. Wesolowski, Quantifying correlated truncation errors in effective field theory. Phys. Rev. C **100**(4), 044001 (2019)
56. S. Binder et al., Few-nucleon systems with state-of-the-art chiral nucleon–nucleon forces. Phys. Rev. C **93**(4), 044002 (2016)
57. E. Epelbaum. High-precision nuclear forces : Where do we stand? *PoS*, CD2018:006, 2019
58. H. Polinder, J. Haidenbauer, U.-G. Meißner, Hyperon nucleon interactions: a chiral effective field theory approach. Nucl. Phys. A **779**, 244–266 (2006)
59. J. Haidenbauer, S. Petschauer, N. Kaiser, U.-G. Meißner, A. Nogga, W. Weise, Hyperon-nucleon interaction at next-to-leading order in chiral effective field theory. Nucl. Phys. A **915**, 24–58 (2013)
60. H. Kamada, M. Kohno, K. Miyagawa. Faddeev calculation of $^{3}_{\Lambda}$H incorporating 2π exchange ΛNN interaction. Phys. Rev. C **108**(2), 024004 (2023)
61. K. Miwa et al., Recent progress and future prospects of hyperon nucleon scattering experiment. EPJ Web Conf. **271**, 04001 (2022)
62. B. S. Tumeo. Feasibility Study of Λd Elastic Scattering in Data From Photoproduction Off Deuteron. Master's thesis, University of South Carolina, 2021

63. J. Haidenbauer, Exploring the Λ -deuteron interaction via correlations in heavy-ion collisions. Phys. Rev. C **102**(3), 034001 (2020)
64. ALICE Collaboration. Future high-energy pp programme with ALICE. (2020). https://inspirehep.net/literature/1839337
65. B. Pandey et al., Spectroscopic study of a possible Λnn resonance and a pair of ΣNN states using the (e, e'K+) reaction with a tritium target. Phys. Rev. C **105**(5), L051001 (2022)